PHILOSOPHICAL TRANSACTIONS OF THE ROYAL SOCIETY A MATHEMATICAL, PHYSICAL & ENGINEERING SCIENCES

The Influence of Horizontal Circulation on the Supply and Distribution of Tracers [and Discussion]

D. Prandle, C. F. Jago, S. E. Jones, D. A. Purdie, A. Tappin, H. Charnock and J. D. Woods

Phil. Trans. R. Soc. Lond. A 1993 **343**, 405-421
doi: 10.1098/rsta.1993.0055

The influence of horizontal circulation on the supply and distribution of tracers

By D. Prandle[1], C. F. Jago[2], S. E. Jones[2], D. A. Purdie[3] and A. Tappin[3]

[1] *Proudman Oceanographic Laboratory, Bidston Observatory, Birkenhead L43 7RA, U.K.*

[2] *School of Ocean Sciences, University of Wales Bangor, Marine Science Laboratories, Menai Bridge, Gwynedd LL59 5EY, U.K.*

[3] *Department of Oceanography, University of Southampton, Southampton SO9 5NH, U.K.*

[Plate 1]

A theoretical analysis of the mixing associated with (horizontal) advection and dispersion is used to show that the larger scale, longer-term distribution of conservative tracers in the southern North Sea is primarily determined by the residual circulation pattern. Model estimates of this circulation have been substantiated from new year-long high-frequency radar monitoring of flow through the Dover Strait.

Model simulations of the saline balance and for the dissolved metals Cd, Cu, Pb, Zn and Ni are made for the North Sea Project (NSP) survey period, using river and atmospheric inputs specified from the 1987 Quality Status Report. Computed concentrations are in reasonable agreement with measured values (except for lead where losses by rapid adsorption were not included in the model). The flushing time, F_T, of the southern North Sea (to 56° N) is approximately 240 days. For any conservative tracer and this value of F_T, the observed seasonal amplitude in concentration corresponding to a seasonal inflow $I \cos wt$ is only 0.23 of the steady concentration corresponding to a continuous inflow I.

By contrast with the above responses for 'conservative' tracers entering from rivers or adjacent seas, concentrations of certain 'non-conservative' tracers can be almost entirely determined by localized exchange processes. Thus the spatial pattern of seasonal variability in temperature and dissolved oxygen is shown to be closely correlated with the inverse of water depth. For such tracers, the influence of advection is small and generally confined to coastal or stratified waters. For shorter term processes, this influence of advection is further reduced.

The transport of suspended sediments is highly dependent on particle size. While the transport of fast-settling sediments is complicated by periodic episodes of settlement and re-suspension, transport of slow-settling sediments (the main agent for adsorbed contaminants) approximates that of a dissolved tracer.

Thus, to first order, simple models incorporating residual advection are adequate to relate inputs to concentrations (averaged over appropriate time and length scales) for reasonably conservative dissolved tracers. Likewise point-models are often adequate to study processes fundamentally concerned with vertical exchange rates particularly for shorter-term processes in well-mixed waters away from the coastal zone.

Phil. Trans. R. Soc. Lond. A (1993) **343**, 405–421
Printed in Great Britain

1. Introduction

A major aim of the North Sea Project (NSP) was the measurement of the distribution of various tracers over an annual cycle. This paper examines simple analytical solutions that approximate these observed annual distributions to provide: (i) a first-order evaluation of these measurements; and (ii) an explanation as to the effectiveness and limitations of simplistic modelling simulations. A particular aim is to clarify why, for certain applications, two-dimensional (2D) (vertically averaged) models simulating horizontal advection and dispersion are used whereas for other applications one-dimensional (1D) (single-point) models simulating only vertical dispersion are used.

Observed tracer concentrations represent the combined effects of both advection and dispersion from the original input together with subsequent addition and depletion from internal and external sources and sinks. We examine how both horizontal and vertical components of these mechanisms determine distributions for both 'conservative' and 'non-conservative' tracers.

In §2, the relative influence of advection and dispersion are examined theoretically. In §3, the horizontal residual circulation computed from a numerical model is described and compared with new measurements of net flow through the Dover Strait. Simulations of the spread of 'conservative' tracers from major rivers, in §4, illustrates how this circulation determines the observed concentrations of salt, dissolved cadmium, copper, lead, zinc and nickel. Section 5 examines the distribution of 'non-conservative' tracers where source or sink terms arise from atmospheric and benthic exchanges. Examples are shown of the seasonal cycle of oxygen and temperature. Section 6 describes progress in simulating the transport of suspended sediment.

2. Advection and dispersion

This section is concerned with the relative importance of advection and dispersion in 2D (vertically averaged) flows. To first determine when vertical variability can be neglected, §2*a* deduces the vertical concentration profile for a cyclical surface exchange Ie^{iwt}. (This result is used later (§5) for applications where vertical variability is of primary interest.) Section 2*b* introduces the flushing time concept, based on horizontal exchanges, to compute area-averaged concentrations for both continuous and cyclical inputs. Section 2*c* develops this flushing time concept to differentiate the stages in mixing during which dispersion and advection predominate.

The equation of conservation of mass, in two orthogonal horizontal dimensions x and y is

$$\frac{\partial C}{\partial t}+U\frac{\partial C}{\partial x}+V\frac{\partial C}{\partial y}=\frac{\partial}{\partial x}K\frac{\partial C}{\partial x}+\frac{\partial}{\partial y}K\frac{\partial C}{\partial y}+\text{sources}-\text{sinks}, \tag{1}$$

advection dispersion

where C is concentration, t is time, U is velocity in the x direction, V is velocity in the y direction and K is a horizontal dispersion coefficient.

Equation (1) is widely used to simulate mixing in shelf seas subject to the assumption of vertical homogeneity. Thus it is necessary to determine the range of conditions for which tracer distributions will be sensibly uniform through the water depth.

(*a*) *Vertical Structure*

In general vertical velocities are small and the effect of vertical advection can be accounted for within the vertical dispersion coefficient K_z. For equation (1) without advective terms and applied to the vertical dimension Z the general solution for a cyclical surface exchange Ie^{iwt} is

$$C(Z,t) = \frac{bI}{iw}\frac{e^{bZ}+e^{-bZ}}{(e^{bD}-e^{-bD})}e^{iwt} \tag{2}$$

(with K_z constant and $\partial C/\partial Z = 0$ at the bed $Z = 0$), where D is the water depth and $b = (iw/K_z)^{\frac{1}{2}}$.

Figure 1*a*, *b* shows, respectively, the amplitude and phase of $C(Z,t)$ at the surface normalized against the depth averaged value, for a range of values of both K_z and D with w taken as an annual cycle.

In many areas of the southern North Sea, where strong tidal action ensures $K_z > 10^{-2}$ m^2 s^{-1}, since $D < 100$ m, vertical homogeneity for the annual cycle is sensibly maintained. However, in areas with weaker tides, thermal stratification can greatly reduce the effective depth-averaged value of K_z (Simpson & Hunter 1974). For a shorter period event of P days duration, the response is equivalent to a dispersion coefficient K_z reduced by $P/365$ in figure 1. Hence, vertical variability is likely to be of primary concern where inputs are concentrated within a period of a month or less.

(*b*) *Flushing time F*

The rate of horizontal exchanges within regions of a sea is often characterized by specification of a flushing time F, where this is the time required for an initial mass (within a bounded region) to reduce to a factor 1/e. Thus

$$C(t) = C_0\, e^{-t/F}. \tag{3}$$

Consider a bounded region of volume V, with a cyclical input $I\cos wt$ and an external exchange rate $-VC/F$ (from (3)), then

$$\frac{dC}{dt} = \frac{I}{V}\cos wt - \frac{C}{F}. \tag{4}$$

For $C = 0$ at $t = 0$ Laplace transforms provide the solution

$$C(t) = \frac{FI}{V(1+F^2w^2)}\{\cos wt + Fw\sin wt - e^{-t/F}\}. \tag{5}$$

For the case of a steady inflow $w \to 0$ and thus (5) gives

$$C(t) = \frac{FI}{V}\{1 - e^{-t/F}\}. \tag{6}$$

For the case of a tracer with an exponential decay rate $e^{-t/\beta}$ (e.g. radioactive decay), F in (5) and (6) is modified to

$$F' = \left\{\frac{F\beta}{F+\beta}\right\}. \tag{7}$$

Figure 2 shows the response of the function (5) in the form of the amplitude (as a

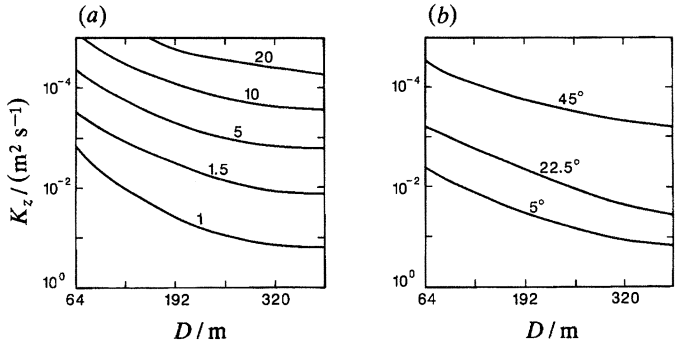

Figure 1. Ratio of surface to depth-mean concentration for a sinusoidal annual cycle of surface exchange. (*a*) Amplitude and (*b*) phase advance. K_z vertical diffusion coefficient, D water depth.

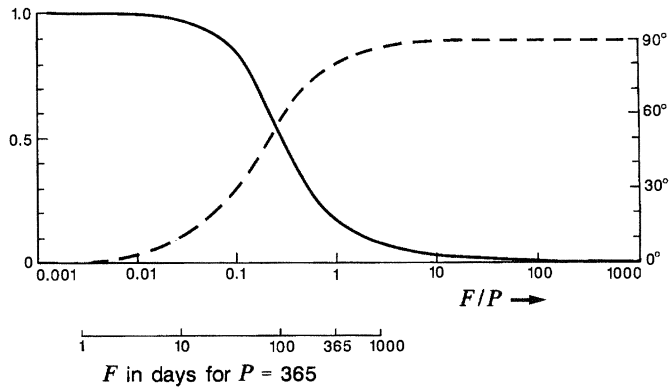

Figure 2. The concentration for a cyclical input $I\cos(2\pi t/P)$ into an area of volume V and flushing time F. Continuous line shows amplitude as a fraction of the steady-state value, FI/V, and the dashed line the phase lag.

fraction of the steady state value (6)) and phase for frequency w. For an annual exchange cycle and $F = 1$ year, the amplitude of the input source will be reduced to 0.16 and a phase lag (relative to the input) of 81° occurs. Conversely for $F < 10$ days, the amplitude will be little changed (from (6)) and the phase lag will be less than 10°. These responses change rapidly for 30 d $< F <$ 100 d.

(*c*) *Flushing due to advection and dispersion*

Advection

For the case of a uniform steady velocity U aligned with the axis of a bounded region of length R, the flushing time associated solely with advection F_A is

$$\left.\begin{aligned} F_A &= R/U, \\ \text{because} \qquad \mathrm{d}C/\mathrm{d}t &= -UC/R = -C/F_A. \end{aligned}\right\} \tag{8}$$

Dispersion

Assuming vertical homogeneity, a tracer of mass M released at time $t = 0$ into an infinite sea of constant depth D will have a distribution, satisfying (1),

$$C(R,t) = (M/4\pi DtK)\exp(-R^2/4Kt), \tag{9}$$

where R is the radial distance from the point of release.

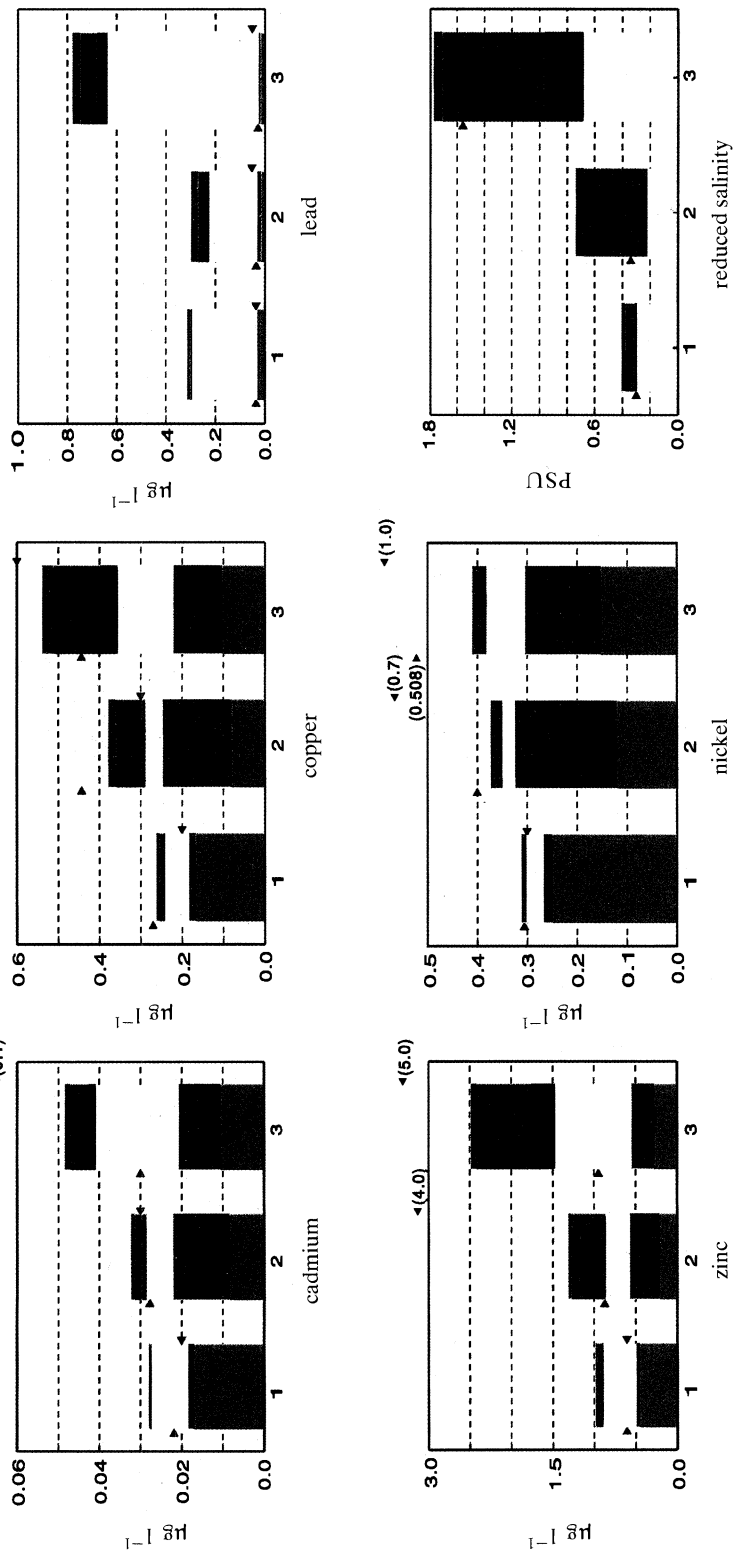

Figure 6. Comparison of annual-mean concentations in sub-regions 1, 2 and 3 (figure 3) obtained from: (i) model simulation, coloured columns, (ii) left arrow ▶ NSPS, (iii) right arrow ◀ 1987 Quality Status Report. Simulation used QSR data for river and atmospheric inputs, NSPS concentrations for boundary inflows.

For $R^2 < 0.4Kt$, $\exp -R^2/4Kt \to 1$ and hence

$$\mathrm{d}C/\mathrm{d}t = -C/t. \tag{10}$$

Hence the 'flushing time' associated solely with dispersion, F_D, is equal to the elapsed time for $t > 2.5R^2/K$, and for this condition

$$F_D > 2.5R^2/K. \tag{11}$$

Advection versus dispersion

The ratio of the effectiveness of these two processes, dispersion:advection, in mixing contaminants is generally represented by the Peclet number Pe where

$$Pe = K/UR. \tag{12}$$

Since the rate of mixing is inversely related to flushing time, a Peclet number can be calculated from (8) and (11)

$$Pe = \frac{F_A}{F_D} = \frac{KR}{2.5R^2U} = \frac{K}{2.5UR} \quad (\text{for } R < 0.6(Kt)^{\frac{1}{2}}). \tag{13}$$

From the southern North Sea, Prandle (1984) found $K \approx 300\ \mathrm{m^2\ s^{-1}}$ and residual velocities typically $1\ \mathrm{cm\ s^{-1}}$. Thus, mixing rates (and flushing times) will be determined by advective processes when

$$R \gg K/2.5U \approx 12\ \mathrm{km}, \tag{14}$$

provided the elapsed time since discharge $t > 14$ days.

3. Residual circulation

(*a*) *Streamline distributions*

Evidence on the net residual circulation in the North Sea has been accumulated over the last century using salinity distributions, current meters, drifting buoys, submarine and telephone cables (to measure induced voltages across channels), radionuclide tracers and, most recently, numerical models. Lee & Ramster (1981) summarized these observational results into a coherent pattern. Subsequent numerical modelling studies by Maier-Reimer (1977), Pingree & Griffiths (1980) and Prandle (1984) have both substantiated and quantified this observed pattern. Figure 3 shows the long-term average streamline distribution calculated by Prandle. These residual flow streamlines are a summation of separate components associated with nonlinear tidal effects and wind forcing. This time and depth-averaged circulation conceals significant variability: residual flows change markedly during large storm events and density gradients can generate significant vertical structure. Likewise, smaller scale flow features can occur intermittently along density fronts or estuarine plumes and persistently from bathymetric features such as gyres off headlands.

For a steady wind having a component W towards the North East, the streamline values ψ shown are modified to ψ^*, where

$$\psi^* = 0.5\psi(1 + (\tfrac{1}{5}\mathrm{W})^2), \tag{15}$$

i.e. the values shown are approximately half due to tidal residuals and one half due to the long-term mean wind speed component of approximately $5\ \mathrm{m\ s^{-1}}$ towards the North East.

PHILOSOPHICAL TRANSACTIONS OF THE ROYAL SOCIETY A MATHEMATICAL, PHYSICAL & ENGINEERING SCIENCES

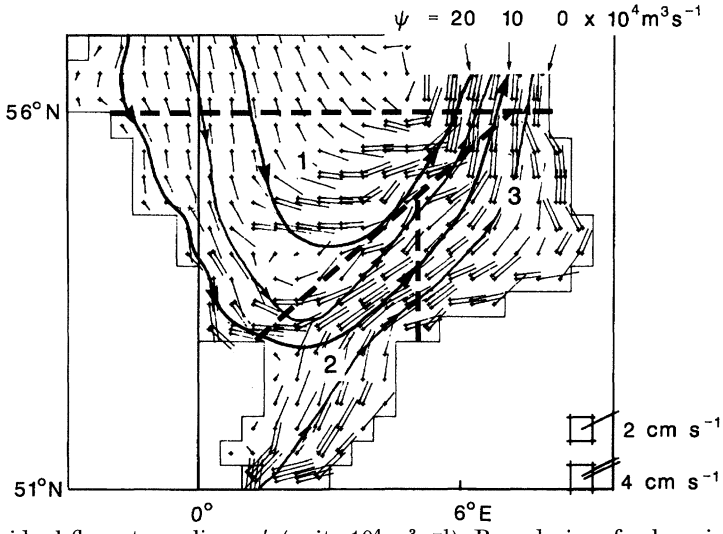

Figure 3. Residual flow streamlines, ψ (units 10^4 m^3 s^{-1}). Boundaries of sub-regions 1 (Central North Sea), 2 (Dutch Coastal) and 3 (German Bight). Region 4 encompasses 1, 2 and 3.

(*b*) *High-frequency radar measurements of flow through the Dover Strait*

In view of the importance of the flow through the Dover Strait on North Sea water quality, year-long measurements to determine the flux of contaminants were made as part of the NSP. Results presented here will be confined to the flow measurements made by shore-based high-frequency (HF) radar, further details of the contaminant fluxes are presented by Burton *et al.* (1993).

The Dover Strait is some 34 km wide with depths of up to 60 m. There has been a long history of attempts to quantify the flow by: (i) direct marine observations (Carruthers 1935; Van Veen 1938; Doodson 1930; Cartwright 1961); (ii) by inference from tracers (Fedorov 1967; Kautsky 1973); (iii) by measurements of induced cross-channel potential differences (Longuet Higgins 1949; Bowden 1956; Cartwright & Crease 1963; Alcock & Cartwright 1977); and (iv) by modelling (Nihoul & Ronday 1975; Pingree & Griffiths 1980; Prandle 1984). Recent developments in the use of land-based HF radar for measuring sea surface currents provide an entirely new approach (Prandle 1991).

Surface currents through the Strait were measured from June 1990 until July 1991 using an HF radar system operating for 6 months from France and for 5 months from England (figure 4). The system measured surface current vectors at 700 pre-selected locations at 20 min intervals, with a range of up to 25 km and a spatial resolution of order 1 km.

Tidal currents

Tidal analysis of separate monthly datasets produced consistent results for the major constituents. In addition to this self-consistency in time, consistency in space was checked by comparison between adjacent values. Thus accurate ellipse data have been compiled at the 159 locations shown in figure 4. Broad agreement was found with comparable data from (i) current meter moorings, (ii) induced voltages on cross-channel telephone cables and (iii) numerical model simulations. A single-point numerical model provided depth-integration subject to the specification of a (constant) eddy viscosity and a bed-stress coefficient. Tidal current profiles measured

PHILOSOPHICAL TRANSACTIONS OF THE ROYAL SOCIETY A MATHEMATICAL, PHYSICAL & ENGINEERING SCIENCES

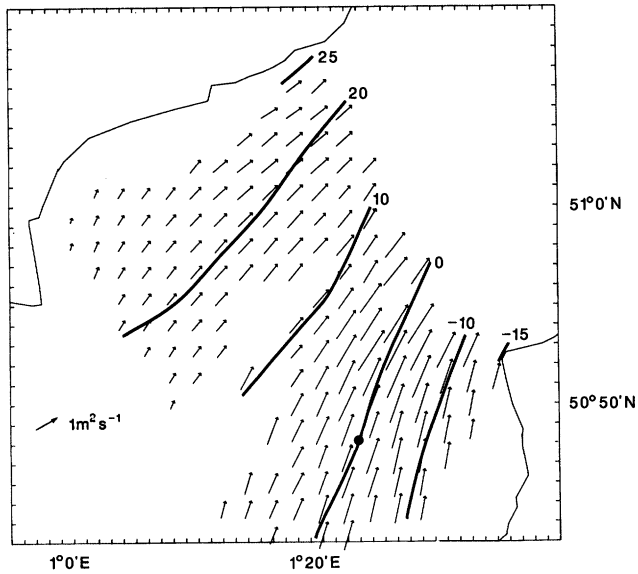

Figure 4. HF radar measurements of the residual M_2 tidal flow through the Dover Strait. Contours indicate streamlines in units of 10^3 m^3 s^{-1} relative to the arbitrary datum. Arrows indicate depth-integrated transports.

from a bottom-mounted acoustic Doppler current profile (ADCP) provided a basis for specifying these parameters. For horizontal integration, spatial harmonic functions were used to fit streamline distributions.

The net residual flow, S_T, over a tidal cycle associated with the M_2 tidal current $(\hat{U}, \theta)$ (confined to one direction) and elevation $(\hat{\zeta}, g)$ in water depth D is

$$S_T = \frac{1}{P}\int_0^P \hat{U}\cos(\omega t-\theta)(D+\hat{\zeta}\cos(\omega t-g))\,\mathrm{d}t = \tfrac{1}{2}\hat{U}\cos(\theta-g). \tag{16}$$

Figure 4 shows the spatial distribution and net value of S_T, this net value of 40000 m^3 s^{-1} is consistent with model simulations carried out with suitably fine resolution (Prandle *et al.* 1993). Likewise the net M_2 tidal flux and net M_2 tidal energy flux were determined. While coarse grid models simulate both the tidal elevation and current amplitudes with reasonable accuracy, much finer resolution is necessary to reproduce the phase delay between these parameters with sufficient accuracy for determination of residual fluxes.

Non-tidal currents

Further analyses of the non-tidal components of observed surface currents are described by Prandle & Player (1993). Components identified include (i) a localized wind-forced drift approximately 20° to the right of the wind direction, (ii) a persistent residual gyre of approximately 20 km diameter off Cap Gris Nez (figure 5), (iii) an axial flow through the Straits associated with large-scale, time-integrated wind forcing and (iv) major oscillations in this axial flow with periods between 20 and 30 h. In addition to the net tidal residual flow of 40000 m^3 s^{-1} and the net long-term wind driven flow estimated as 60×10^3 m^3 s^{-1}, a remaining long term eulerian residual current contributed an estimated 10000 m^3 s^{-1}. Thus the net long term flux was estimated as 110000 m^3 s^{-1}.

PHILOSOPHICAL TRANSACTIONS OF THE ROYAL SOCIETY A MATHEMATICAL, PHYSICAL & ENGINEERING SCIENCES

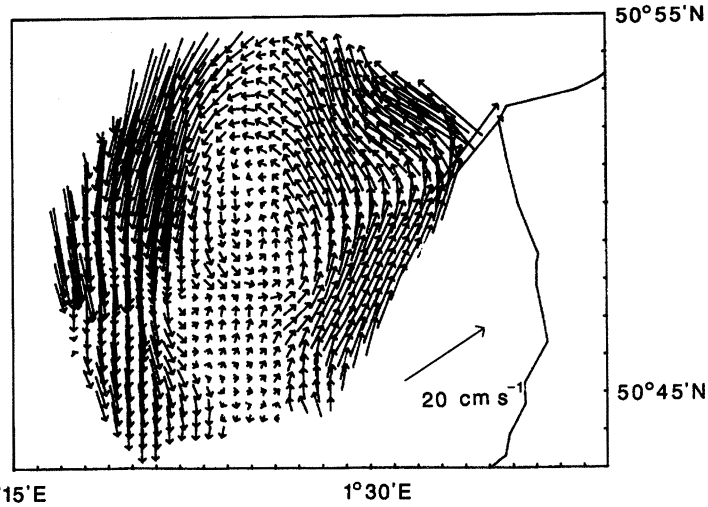

Figure 5. Monthly averaged residual surface currents after removal of the wind-driven and tidal components.

4. Mixing of fresh water and dissolved metals

The Proudman Oceanographic Laboratories' general purpose two-dimensional (vertically averaged) 35 km grid numerical model was run with long-term mean residual flows (figure 3) to reproduce resultant distributions in the southern North Sea of tracers discharged from (i) the Tyne and the Tees, (ii) the Humber, (iii) the Thames, (iv) the Scheldt, Rhine and Meuse, (v) the Ems, Weser and Elbe and originating from (vi) the Dover Strait, (vii) the northern North Sea and (viii) deposited from spatially uniform rainfall. Flushing times for sections of the North Sea were calculated by initially specifying a uniform concentration in the section and then determining the time for this initial mass to reduce to a fraction $1/e$.

For convenience in discussing results from these model simulations, the North Sea south of 56° is divided into three sub-regions (shown in figure 3), namely (1) the Central North Sea, (2) the Dutch coastal zone and (3) the German Bight. These sub-divisions were selected by reference to (i) streamline orientation, (ii) proximity to major river inflows and (iii) the size criterion of equation (14) for advective transport to predominate in determining mean concentrations. Fortuitously, these three regions coincide closely with areas for which data are published in the 1987 Quality Status of the North Sea report (QSR).

Table 1 shows the volumes, flushing times and percentage water mass compositions (as a function of source) computed for these sub-regions. Clearly the shelf sea circulation overwhelmingly determines the net composition with water from the English Channel constituting, respectively, in region 1, 5%; region 2, 52%; region 3, 38%; region 4, 19%. Water from the northern North Sea effectively constitutes the remainder, except river discharges from the Scheldt and Rhine amount to 1.3% in region 2 (Dutch Coastal) and 2% in region 3. Rainfall constitutes between 0.6 and 0.9% except in region 3 (German Bight) where it is almost 2%.

The flushing times vary from 72 days for region 3 to 240 days for region 4 (the entire area south of 56° N). Thus, from §2*b*, seasonal variability in the source terms is likely to be significantly reduced when concentrations are averaged over these regions. However some significant component should remain in region 3, especially

Table 1. *Volume, flushing time and percentage mass composition for four regions*
(Region 1, central North Sea; region 2, Dutch Coastal; region 3, German Bight; region 4, southern North Sea.)

		region 1	region 2	region 3	region 4
volume/(km^3)		5990	1830	960	8780
flushing time/days		196	108	72	240
source	$Q/(10^6\ m^3\ day^{-1})$	percentage mass composition			
Tyne/Tees	5.4	—	—	—	—
Humber, Wash	16.4	0.1	0.1	0.2	0.1
Thames	5.8	—	—	—	—
Scheldt, Rhine, Meuse	271	0.2	1.3	2.1	0.6
Weser, Ems, Elbe	152	—	—	0.8	0.1
rainfall	2.67 mm day^{-1}	0.8	0.6	1.9	0.9
Dover Strait	—	5.1	52.4	38.4	18.6
Northern Boundary	—	93.8	45.6	56.6	79.7

Table 2. *Annual inputs of dissolved metals from rivers and atmospheric deposition observed (NSPS) and simulated masses in region 4*

	annual input/tonnes					
	Cd	Cu	Pb	Zn	Ni	H_2O
UK[a] rivers	6	142	165	415	161	10×10^9
Netherlands[a] rivers	21	535	343	3055	N/A	99×10^9
Germany[a] rivers	12	288	257	2088	N/A	55×10^9
atmosphere[b]	240	1600	7400	11000	950	—
Dover Strait	90	1090	101	2380	1360	—
Total	369	3655	8266	18938	2471	164×10^9
mass in region 4						
NSP survey[c]	220	3190	290	6500	3320	130×10^{9d}
model simulation	272	2773	3167	10740	2940	119×10^9
F[e]	217	319	13	125	490	289

[a] Data from *Quality status of the North Sea* (*Proc. Second Int Conf on Protection of the North Sea.* HMSO.)
[b] Atmospheric inputs correspond to high estimate all deposited south of 56° N.
[c] Mass within survey area (south of 56° N).
[d] Assumes the difference between the mean observed salinity of 34.245 psu and that at the north-east boundary 34.768 psu reflects the proportion of fresh water.
[e] F (days) = NSP survey mass (in region 4) × 365/total inputs = flushing time for region 4.
N/A: not available.

for sources from the Rhine, Scheldt and Elbe. Although, as indicated by the theory, seasonal peaks off-shore may be up to 3 months after the peak at the discharge point (possibly longer allowing for transit time of distant sources).

(*a*) *Salt*

Table 2 shows the net annual freshwater inflow from the major rivers discharging into the southern North Sea amounts to 164×10^9 tonnes. An exact balance is assumed between the annual rainfall (of approximately 1 m) and evaporation. An estimate of the net freshwater content in region 4 was obtained by using spatial and temporal

(averaged over 15 monthly surveys) salinity data from the North Sea Project Survey (NSPS). The difference between this mean value, 34.245 PSU, and the mean along the inflow region of the Northern boundary of the model, 34.768 PSU, was assumed to represent the freshwater content, i.e. 130×10^9 tonnes. Some refinement of this estimate was made by allowing for the reduced mean salinity observed along the Dover Strait boundary (34.694‰), however this is found to be of secondary importance. From the ratio of these two quantities a flushing time of 289 days is calculated compared to the model derived value of 240 days shown in table 1. However, this latter flushing time (i) assumes a mass initially uniformly distributed in region 4, and (ii) neglects recirculation of material back into this southern section of the North Sea. Some inaccuracy in the inflow data must also be expected. Figure 6 compares these computed salinities against the NSPS observed data for the three sub-regions and also indicates contributions from differing sources. Overall, the level of agreement found is encouraging for the compatibility of (i) the NSPS data, (ii) the QSR inflow data and (iii) the model simulation.

(*b*) *Dissolved metals*

The simulation described for freshwater discharges mixing in the southern North Sea was repeated for the dissolved components of the metals: cadmium, copper, lead, zinc and nickel. Net river and atmospheric discharges were obtained from the QSR, in all cases the 'high' estimate was adopted. Concentrations along the open boundaries of the model were specified from mean values over the four NSP surveys on which dissolved metal concentrations were made (Burton *et al.* 1993).

Resulting concentrations for each of the three sub-regions are shown in figure 6. This figure shows the proportional source contributions and includes: (i) the mean (spatially averaged and over the four surveys) NSPS observed data and (ii) concentrations cited in the QSR. The simulations all assume conservative tracers. Discussion of results will be confined to values over the entire southern North Sea (region 4) listed in table 2.

Cadmium

The computed concentrations comprise fractions of 0.47 from the northern boundary, 0.16 from the Dover Strait and 0.37 from river and atmospheric sources. Thus the reasonable agreement between observed and computed concentrations adds confidence to both the estimates of net sources and to the model exchange rate. The calculated flushing time of 217 days is close to the modelled value of 240 days (table 1). The relatively high observed concentration on the northern inflow boundary (0.018 μg dm^{-3}, compared with the observed spatial mean value of 0.025 μg dm^{-3}) indicates a significant northerly source of cadmium.

Copper

The fractional composition of copper is similar to that for cadmium although the Dutch inflows are larger for copper. The overall level of agreement between observed and model concentrations is also similar to that for cadmium although, in this case, the model value is less than the observed. The calculated flushing time of 319 days combined with the model underestimate of mean concentration, suggests that the QSR estimate of inflows may be underestimated.

PHILOSOPHICAL TRANSACTIONS OF THE ROYAL SOCIETY A MATHEMATICAL, PHYSICAL & ENGINEERING SCIENCES

Lead

A fraction 0.80 of the computed lead concentrations is due to atmospheric deposition. Computed concentrations are an order of magnitude higher than observed. Unless these atmospheric deposition rates are substantially overestimated, this discrepancy can be attributed to the omission from the model of the rapid loss of dissolved lead to the particulate phase (Balls 1989).

Zinc

A fraction of 0.58 of the computed zinc concentration is from river and atmospheric sources. The computed concentrations are almost double NSPS observations but lower than the QSR values, possibly indicating that QSR inputs and concentrations were overestimates of 1989–1990 conditions. The calculated flushing time of 125 days taken in combination with indications of overestimates of the direct inputs, might also indicate a significant loss of zinc from the dissolved phase.

Nickel

With discharges from the Elbe and Rhine omitted from this simulation, river and atmospheric inputs account for only 0.15 of the computed concentrations. Thus the lower mean value of the computed concentrations relative to the NSPS observations might be related to these omissions. Indications from the QSR of raised concentrations in the German Bight reinforce this deduction. Inclusion of inputs from these two sources would also lower the computed flushing time of 490 days.

Summary

These simulations indicate first order consistency between: (i) QSR estimates of river and atmospheric input, (ii) both QSR and NSPS observed concentrations and (iii) model exchange rates. An exception occurs for lead, where rapid loss from the dissolved phase must be invoked to account for the imbalance between the direct inputs and the observed concentrations. While more detailed simulations are required to incorporate interactions with those dissolved tracers, this preliminary study has illustrated the usefulness of a simple model that primarily reproduces the effect of horizontal circulation. The computed flushing times are lowest for lead (13 days) followed by zinc (125 days). From (7) such reductions in F can be an indication of significant 'decay' rates. Balls (1989) lists all of the metals considered here in order of their partition coefficient, K_d, values (quantifying the rate of adsorption onto particulates). Balls shows the largest value of K_d is for lead, and the next largest is zinc.

For conservative tracers, simple models reproducing horizontal circulation can be used to accurately relate concentrations to inputs, provided appropriate scales for temporal and spatial averaging are incorporated.

5. Mixing of non-conservative tracers

Mathematically, three forms of the 'non-conservative' nature of tracers can be readily identified, namely: (i) exponential decay as for radio-active material; (ii) atmospheric or benthic exchange; and (iii) dynamic interaction dependent on the

concentration of other parameters e.g. biological grazing. In case (i), from equation (7) a half life of β reduces the flushing time F in the ratio $\beta/(F+\beta)$. Solar heating and surface cooling primarily determine temperature in shallow shelf seas and hence the seasonal cycle of temperatures is examined as an example of case (ii). Likewise, benthic uptake of oxygen can similarly be examined under case (ii). While dynamic interactions are beyond the scope of present interest, complex processes such as the annual plankton cycle may be strongly influenced by the supply of a tracer determined by advective transport.

(*a*) *Atmospheric and benthic sources and sinks*

For tracers in case (ii), the question arises as to the importance of advection relative to the surface or bed exchange rates. From equation (2) the depth-averaged concentration resulting from a (spatially homogeneous) atmospheric or benthic input (or output) $I\,\mathrm{e}^{\mathrm{i}wt}$ is

$$\bar{C}(t) = (I/\mathrm{i}Dw)\,\mathrm{e}^{\mathrm{i}wt}. \tag{17}$$

To first order the (depth-averaged) advection along the x axis is

$$-(UI/\mathrm{i}D^2w)\,\mathrm{e}^{\mathrm{i}wt}\,\partial D/\partial x. \tag{18}$$

Thus the relative influence of advection: this source term in (1) is

$$U\frac{\partial D/\partial x}{D} : w. \tag{19}$$

For the seasonal cycle $w = 2\times10^{-7}\ \mathrm{s}^{-1}$. Thus for $U = 0.01\ \mathrm{m\ s}^{-1}$, this source term is relatively unaffected by advection when the distance over which the depth changes by a factor of 2 is greater than 100 km. In the deeper offshore sections of the southern North Sea, this relevant length scale is greater than 100 km and hence there is a localized balance for spatially uniform atmospheric and benthic inputs. Conversely in the near-coastal regions this length scale is less than 100 km and hence advection modifies the spatial distribution of the seasonal cycle in coastal areas. (Note that advection of other source terms can be important in all regions.)

Conversely for a much shorter period atmospheric input, advection by residual currents is likely to be unimportant (except in coastal regions). As an example, for the tranquil clear-sky conditions conducive to plankton blooms, residual circulation is likely to be a secondary influence (although tidal advection and vertical structure may be important).

(*b*) *Oxygen*

The combined influences of horizontal circulation and a benthic sink were evident in a preliminary simulation of the annual cycle of dissolved oxygen. (Subsequent simulation results are shown in Huthnance (1993).) The simulation commenced in March with 100% saturation level, a 'benthic' oxygen sink was then specified equal to $0.5D\%\ \mathrm{m}^{-3}\ \mathrm{day}^{-1}$. Advective velocities were prescribed as in §3. Figure 7*a* shows the computed saturation levels in August, indicated as percentage oxygen sag. The area of maximum depletion in the German Bight corresponds with an observed hypoxic 'stress' region where under conditions of summer thermal stratification oxygen depletion has been measured in near bottom waters (Howarth *et al.*, this volume). While the effect of this assumed depletion mechanism is clearly inversely correlated with the depth contours (figure 7*b*), the additional impact of advection in

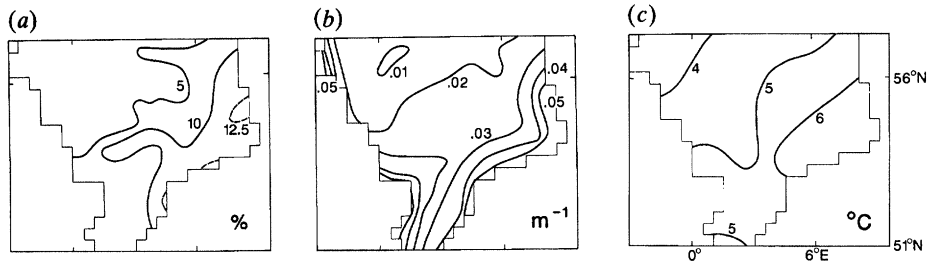

Figure 7. (*a*) Percentage sag in dissolved oxygen saturation computed for August as a result of uniform benthic demand from 100% saturation in March. (*b*) $1/D$, D water depth in metres. (*c*) Amplitude of the annual cycle of observed sea surface temperatures.

shallow regions is also evident from this simulation. The added effect, whereby seasonal thermal stratification in deeper waters limits surface exchanges, is not represented in this simple simulation model.

(*c*) *Temperature*

The annual cycle of sea surface temperature $\bar{T}_s + \hat{T}_s \cos(wt - gs)$, for a well mixed sea determined solely by localized balance is (Prandle & Lane 1993)

$$T_s(t) = \bar{T}_a + \frac{\bar{S}}{K} + \frac{\hat{S}\cos wt + k\hat{T}_a \cos(wt - ga)}{(k^2 + \alpha^2 D^2 w^2)^{\frac{1}{2}}}, \tag{20}$$

where $\bar{S} + \hat{S}\cos wt$ is the effective solar radiation term, $\bar{T}_a + \hat{T}_a \cos(wt - ga)$ the ambient air temperature, α the thermal capacity of water, and $k(T_a - T_s)$ the rate of surface heat loss. In general $\hat{S} \ll \hat{T}_a k$ and thus in shallow water ($D \ll k/\alpha w$), the seasonal amplitude of sea surface temperature, $\hat{T}_s$, is given by

$$\hat{T}_s \to \hat{T}_a. \tag{21}$$

Conversely in deep water ($D \gg k/\alpha w$)

$$\hat{T}_s \to \hat{T}_a\, k/D\alpha w. \tag{22}$$

The annual mean sea surface temperature

$$\bar{T}_s = \bar{T}_a + \bar{S}/K \tag{23}$$

irrespective of depth or the ratio of $\hat{S}{:}\hat{T}_a$.

Figure 7*c* shows the amplitude of the annual cycle of observed sea surface temperatures in the North Sea (extracted from ICES 1978–1982). In the shallow water of the German Bight ($\hat{T}_s, gs$) closely follow the pattern of the annual cycle of air temperature (Korevaar 1990). However, in deeper water, the amplitude is significantly reduced. The extent of this reduction is not as great as indicated by (22) since stratification reduces the thermal exchange with deeper water and thus effectively reduces D in (22).

The time of maximum T_s is nearly coincident throughout the southern North Sea. From figure 1, this might be interpreted as indicating values of $K_z > 10^{-2}\ \mathrm{m^2\ s^{-1}}$. However significant phase lags occur in the lower layers of the deeper stratified water, indicating a much reduced value of K_z in these areas. The response time for complete vertical mixing of a surface thermal exchange is D^2/K_z, i.e. 115 days for $K_z = 0.001\ \mathrm{m^2\ s^{-1}}$ in a water depth of 100 m.

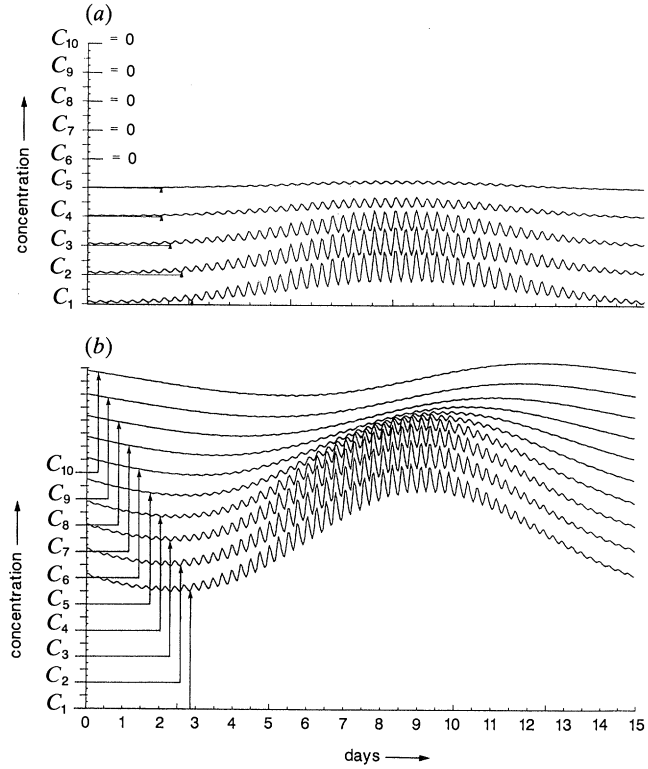

Figure 8. Simulation of suspended sediment concentrations over a 15-day spring-neap tidal cycle. (*a*) $E/DW_s = 0.1$. (*b*) $E/DW_s = 10$. Concentration $C_1, C_2, C_3, \ldots, C_{10}$ at fractional heights 0.05, 0.15, 0.25, ..., 0.95 above the bed. Concentration scale linear but arbitrary. Vertical eddy viscosity E, water depth D, settling velocity W.

The stratification in deeper water invalidates the analysis of §5*a*, observational evidence and 3D modelling results indicate that baroclinic circulation is important in such conditions.

6. Suspended sediments

While suspended particulate matter with low settling velocities W_s may move as if dissolved, i.e. transported by the mean advection and dispersion in equation (1), particles with greater W_s move by a succession of settlement and resuspension cycles. Terrigenous particles of clay, silt and fine sand sizes have $W_s = 10^{-6}$, 10^{-4} and 10^{-2} m s^{-1}, which allows them to fall 10 m in 116 d, 28 h, 17 m respectively. Thus even clay-size terrigenous particles of oceanic origin can undergo some settlement before arrival in the southern North Sea, though they will remain suspended in areas of strong tidal currents or significant wave action. By contrast, silt-size terrigenous particles may be periodically deposited and resuspended over a spring-neap cycle. Sand-size terrigenous particles may only be resuspended over a small part of the semi-diurnal tidal cycle.

In a theoretical analysis of tidally driven sediment transport, Prandle (1993) shows that for $E/DW_s < 0.1$ (E is the vertical eddy diffusivity), suspended sediment particles are concentrated near the bed (figure 8) and hence equation (1) does not apply. Conversely for $E/DW_s > 10$ there is little vertical structure in suspended sediment concentration and equation (1) is applicable. Consequently, these criteria

indicate that transport of particles with small W_s approximates that of a dissolved conservative tracer. Such particles are either clay-rich and/or organic-rich flocs with large specific surface areas and so most effective in the flux of adsorbed contaminants. This analysis does not apply in cases of especially high suspended sediment concentration where the value of E is partly determined by these sediments (cf. Jago *et al.* 1993).

Numerical models are required to determine the transport rates of particles with faster settling rates. In the process, some empirical re-suspension formulae must be assumed or, preferably, such formulae can be deduced by comparison of computed model results with observational data. Recent development of acoustic Doppler current profiler (ADCP) instruments are ideal for this purpose (Jones *et al.* 1993) since they can provide a continuous time series of the vertical profile of suspended sediments. Conversion of the back-scatter signal amplitude to a suspended sediment concentration is complicated by the dependency on particle size. However, where the sediment movement is effectively by tidal currents, the characteristics of vertical profiles of tidal resuspension time-series are so dependent on the effective value of W_s (figure 8) that modelling simulations can be used to infer W_s. By combining the latter with observational techniques for identifying particle types it is then possible to infer particle size spectra.

7. Conclusions

Theoretical analyses of the effects of advection and dispersion on the NSP tracer observations indicate that the distribution of conservative tracers is primarily determined by the residual horizontal circulation with advection predominating over dispersion on space scales greater than $O(10\text{ km})$. Model simulations of this circulation were verified against: (i) new year-long (HF radar) measurements of flow through the Dover Strait and (ii) observed distributions of salt, cadmium, copper, lead, zinc and nickel from the NSP survey. The accuracy of these simulations also encourages confidence in the accuracy of the specified river and atmospheric inputs (extracted from the 1987 QSR) and in the dissolved concentrations cited in the QSR. (The anomalous result found for lead was attributed to its known high particle affinity.)

By contrast concentrations of the 'non-conservative' tracers oxygen and temperature are shown to be determined more by localized conditions and thus are more dependent on water depth than advective circulation.

The amplitude of seasonal variations averaged over the southern North Sea is substantially reduced because of its slow flushing rate: a flushing time of 240 days was calculated for the area between the Dover Strait and 56° N. This long flushing time is the result of small residual velocities, $O(1\text{ cm s}^{-1})$. These small velocities do not readily smear short term, small scale episodic atmospheric exchanges, thus possibly enhancing patchiness and 'bloom' conditions; especially in regions of small tidal advection.

The transport of suspended sediment concentrations is highly dependent on settling velocity and particle size. However, adsorbed contaminants are primarily associated with slow settling particles for which the transport approximates that of a dissolved conservative tracer with concentrations determined by residual circulation. Conversely, transport of faster settling particles is via a series of resuspension and settlement sequences and thus observed concentrations reflect the precise tidal, wind and wave conditions pertaining.

PHILOSOPHICAL TRANSACTIONS OF THE ROYAL SOCIETY A MATHEMATICAL, PHYSICAL & ENGINEERING SCIENCES

Exceptions to these general conclusions apply in near-coastal, near-frontal or highly stratified areas where physical and biological processes can produce significant variability on small temporal and spatial scales. Thus the effect on contaminant distribution of such features as the persistent residual gyre observed in the Dover Strait or the coastally trapped Rhine water observed along the Dutch coast remain to be considered. For accurate simulation of the 'peak' concentrations that can occur under such conditions, a high resolution, fully 3D, density evolving model is required.

References

Alcock, G. A. & Cartwright, D. E. 1977 An analysis of 10 years' voltage records from the Dover-Sangatte cable. In *A voyage of discovery, George Deacon 70th Anniversary volume* (ed. M. Angel), pp. 341–365. Oxford: Pergamon Press.

Balls, P. W. 1989 The partition of trace metals between dissolved and particulate phases in European coastal waters: a compilation of field data and comparison with laboratory studies. *Netherlands J. Sea Res.* **23**, 7–14.

Bowden, K. F. 1956 The flow of water through the Straits of Dover related to wind and differences in sea level. *Phil. Trans. R. Soc. Lond.* A **248**, 517–551.

Carruthers, J. N. 1935 The flow of water through the Straits of Dover as gauged by continuous current-meter observations at the Varne lightvessel. Part II. In *Fishery Investigations*, ser II, vol. 14.

Cartwright, D. E. 1961 A study of currents in the Straits of Dover. *J. Inst. Navig.* **14**, 130–151.

Cartwright, D. E. & Crease, J. 1963 A comparison of the geodetic reference levels of England and France by means of the sea surface. *Proc. R. Soc. Lond.* A **273**, 558–580.

Doodson, A. T. 1930 Current observations at Horn's Rev, Varne and Smith's Knoll in the years 1922 and 1923. *J. Cons. perm. int. Explor. Mer* **5**, 22–32.

Fedorov, K. N. 1967 The variability of flow through the Strait of Dover from observations of salinity. *Oceanol.* **7**, 467–471.

Flather, R. A. 1976 A tidal model of the North-west European Continental Shelf. *Mém. Soc. r. Sci. Liege* **10**, 141–164.

Kautsky, H. 1973 The distribution of the radio nuclide Caesium 137 as an indicator for North Sea watermass transport. *Dt. hydrogr. Z.* **26**, 241–246.

Korevaar, C. G. 1990 *North Sea Climate: based on observations from ships and lightvessels*. Kluwer Academic Publishers.

Jones, S. E. *et al.* 1993 Suspended sediment dynamics, their measurement and modelling in the Dover Strait. In *Physical mechanisms of transport and dispersion in the environment* (ed. K. Bevan). John Wiley. (In the press.)

Lee, A. J. & Ramster, J. W. (eds) 1981 *Atlas of the seas around the British Isles*. Ministry of Agriculture, Fisheries and Food. Directorate of Fisheries Research.

Longuet-Higgins, M. S. 1949 The electrical and magnetic effects of tidal streams. *Mon. Not. R. Astrom. Soc., Geophys. Suppl.* **5**, 285–307.

Maier-Reimer, E. 1977 Residual circulation in the North Sea due to the M_2 tide and mean annual wind stress. *D. hydrogr. Z.* **30**, 253–262.

Nihoul, J. C. J. & Ronday, F. C. 1975 The influence of the 'tidal stress' on the residual circulation. Application to the Southern Bight of the North Sea. *Tellus* **27**, 484–489.

Pingree, R. D. & Griffiths, D. K. 1980 Currents driven by a steady uniform wind stress on the shelf seas around the British Isles. *Oceanol. Acta* **3**, 227–236.

Pingree, R. D. & Maddock, L. 1977 Tidal residuals in the English Channel. *J. Mar. Biol. Assoc.* **58**, 965–973.

Prandle, D. 1978 Monthly mean residual flows through the Dover Strait, 1949–1972. *J. Mar. Biol. Assoc.* **58**, 965–973.

Prandle, D. 1984 A modelling study of the mixing of 137Cs in the seas of the European continental shelf. *Phil. Trans. R. Soc. Lond.* A **310**, 407–436.

PHILOSOPHICAL TRANSACTIONS OF THE ROYAL SOCIETY A MATHEMATICAL, PHYSICAL & ENGINEERING SCIENCES

Prandle, D. 1991 A new view on near-short dynamics based on observations from H.F. radar. *Progr. Oceanogr.* **27**, 403–438.

Prandle, D. 1993 The dynamics of suspended sediments in tidal waters. (Submitted.)

Prandle, D. & Lane, A. 1993 The annual temperature cycle in shelf seas. (Submitted.)

Prandle, D. & Player, R. 1993 Residual currents through the Dover Strait measured by H.F. Radar. *Estuar. Coast. Shelf Sci.* (In the press.)

Prandle, D., Loch, S. G. & Player, R. 1992 Tidal flow through the Straits of Dover. *J. phys. Oceanogr.* **23**, 22–37.

Simpson, J. H. & Hunter, J. R. 1974 Fronts in the Irish Sea. *Nature, Lond.* **250**, 404–406.

Van Veen, J. 1938 Water movements in the Straits of Dover. *J. Cons. perm. int. Explor. Mer* **14**, 130–151.

Discussion

H. Charnock (*University of Southampton, U.K.*). Are the results presented valid for stably stratified conditions?

D. Prandle. The results for both the 2D horizontal (vertically averaged) model and the 1D vertical point model break down under such conditions. However, for the southern North Sea, these models are generally valid throughout the winter period and over approximately 70% of the region under summer conditions.

J. D. Woods (*NERC, Swindon, U.K.*). How does the existence of fronts affect the results presented and do the results from the 'frontal experiments' offer evidence thereof?

D. Prandle. This is a fundamental question not entirely resolved (although the paper by Hill *et al.* (this symposium) addresses this question directly). However, models of mixing processes on large (> 30 km) scales in the North Sea appear to be reasonably accurate without any frontal mechanism incorporated.

Colour plate printed by George Over Ltd, London and Rugby.

PHILOSOPHICAL TRANSACTIONS OF THE ROYAL SOCIETY A MATHEMATICAL, PHYSICAL & ENGINEERING SCIENCES

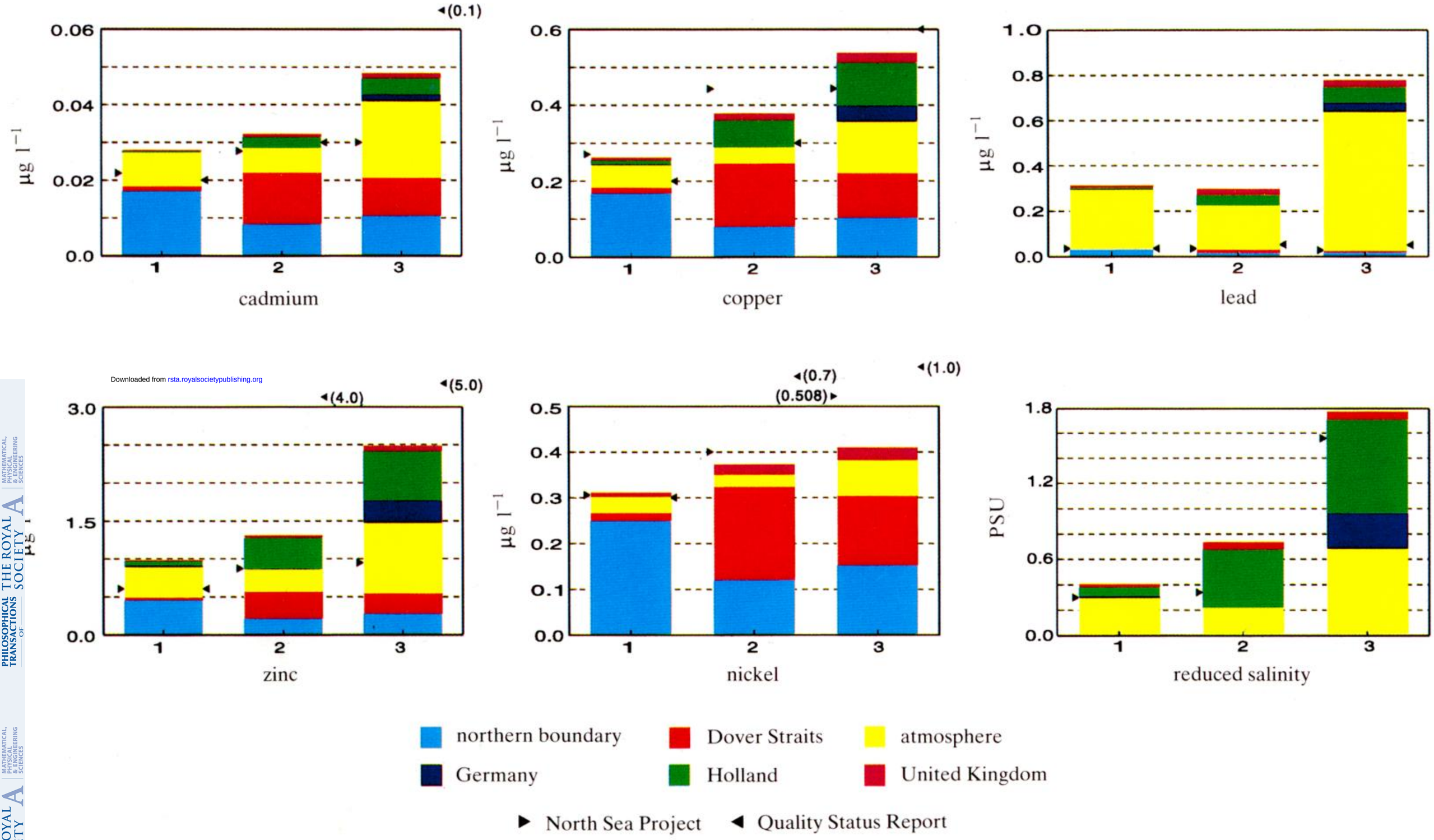

Figure 6. Comparison of annual-mean concentations in sub-regions 1, 2 and 3 (figure 3) obtained from: (i) model simulation, coloured columns, (ii) left arrow ▶ NSPS, (iii) right arrow ◀ 1987 Quality Status Report. Simulation used QSR data for river and atmospheric inputs, NSPS concentrations for boundary inflows.